Cationic Noble Gas Hydrides: A Theoretical Investigation of Dinuclear $HNgFNgH^+$ (Ng = He−Xe)

Stefano Borocci, Nicoletta Bronzolino, Maria Giordani, and Felice Grandinetti*

Dipartimento di Scienze Ambientali, Università della Tuscia, L.go dell' Università, s.n.c., 01100 Viterbo, Italy

Received: March 5, 2010; Revised Manuscript Received: May 19, 2010

Theoretical calculations at the B3LYP, MP2, and CCSD(T) levels of theory disclose the conceivable existence of cationic noble gas hydrides containing two Ng atoms. These species have a general formula of $HNgFNgH^+$ (Ng = He−Xe), and are the cationic counterparts of the neutral HNgF. The optimized geometries, harmonic frequencies, and bonding properties point to ion−dipole complexes between a fluoride anion and two covalent $H-Ng^+$ cations, best formulated as $(H-Ng^+)_2F^-$. The $HXeFXeH^+$ is also isoelectronic with the recently experimentally observed HXeOXeH (Khriachtchev et al. *J. Am. Chem. Soc.* **2008**, *130*, 6114−6118). The resulting $HNgFNgH^+$ are thermochemically stable with respect to dissociation into $HNg^+ + HNgF$ and $HNg^+ + H + Ng + F$, but are largely unstable with respect to both the loss of HF (with formation of $HNg^+ + Ng$) and H_2F^+ (with formation of two Ng atoms). These decompositions pass through bent transition structures, and only the heaviest $HArFArH^+$, $HKrFKrH^+$, and $HXeFXeH^+$ are protected by energy barriers large enough (ca. 10−15 kcal mol^{-1}) to support their conceivable metastability. In line with other series of noble gas compounds, the neon cation $HNeFNeH^+$ is the least stable among the various $HNgFNgH^+$.

1. Introduction

The chemistry of the noble gases is currently enjoying an upsurged interest,[1] stimulated by the recent discovery of unprecedented compounds and bonding motifs.[2−9] The noble gas hydrides HNgY (Ng = noble gas atom; Y = electronegative fragment) constitute in particular a relevant part of modern noble gas chemistry.[10,11] These molecules are prepared by photodissociation of HY in a cold Ng matrix, and their properties and stability are investigated by infrared spectroscopy and theoretical calculations. Already observed species include HArF, the first argon compound,[12,13] and nearly 20 HKrY and HXeY.[11] Interestingly, the family of the noble gas hydrides also includes two dinuclear species, namely HXeCCXeH,[14] and the recently observed HXeOXeH.[15,16] The latter molecule is obtained by photolysis of H_2O/Xe,[15] and it is, to date, the simplest noble gas compound containing two Ng atoms. Neutral compounds containing two Ng atoms have been also investigated by theoretical calculations.[17,18] Cationic noble gas hydrides $HNgY^+$ are generally only little explored, and the $HNgCO^+$ ions (Ng = He−Xe) are a recent theoretical example.[19] In the present study, we discuss one of the first exemplary groups of cationic noble gas hydrides containing two Ng atoms. These species have a general formula of $HNgFNgH^+$ (Ng = He−Xe), and are the simplest ionic counterparts of the extensively investigated HNgF.[12,20−36] The xenon cation $HXeFXeH^+$ is also isoelectronic with the experimentally observed HXeOXeH.[15] We discuss here the properties and stability of the $HNgFNgH^+$ ions, and also make a brief comparison with their neutral analogues HNgF.

2. Computational Details

The ab initio calculations were performed with the Gaussian03 program[37] using the Dunning's correlation consistent double- and triple-ζ basis sets, augmented with diffuse functions (aug-cc-pVDZ and aug-cc-pVTZ)[38] for H, F, He, Ne, Ar, and Kr. The relativistic Stuttgart/Dresden (SDD) effective core potential and the valence basis set designed for this ECP were used for Xe.[39] The presently employed basis sets will therefore be denoted as aug-cc-pVDZ/SDD and aug-cc-pVTZ/SDD. The second-order Møller−Plesset[40] (MP2) and the coupled cluster theoretical method,[41] including the contribution from single and double substitutions and an estimate of connected triples, CCSD(T), were employed within the frozen-core approximation. The density functional theory (DFT) calculations were performed using the hybrid exchange-correlation functional B3LYP, which combines the three terms exchange functional proposed by Becke (B3)[42] with the correlation functional of Lee, Yang, and Parr (LYP).[43] The geometry optimizations and harmonic frequency calculations performed at the MP2, CCSD(T), and B3LYP levels of theory were based on analytic or numerical gradients. The characterization of the critical points as energy minima or transition structures (**TS**) was based on the calculation of their harmonic frequencies, also used to evaluate the zero-point vibrational energies (ZPE). Intrinsic reaction coordinate (IRC) calculations[44] were performed at the MP2 and B3LYP levels of theory to unambiguously relate any **TS** to its interconnected energy minima. The atomic charges were computed by natural bond orbital (NBO) analysis[45] of the MP2/aug-cc-pVTZ/SDD wave function. The dissociation energies were corrected for the effect of the basis set superposition error (BSSE) using the counterpoise method of Boys and Bernardi.[46] Chemical bonding analysis was based on the theory of atoms-in-molecules (AIM),[47] as implemented in the AIM2000,[48] using the MP2/aug-cc-pVTZ/SDD electron density. We calculated in particular, at the MP2/aug-cc-pVTZ/SDD optimized geometries, the charge density ρ, the Laplacian of the charge density $\nabla^2\rho$, and the energy density H at the bond critical points (bcp's), intended as the points on the attractor interaction lines where $\nabla\rho = 0$. In line with the experience of other authors,[24b] we had severe problems in performing the AIM analysis of the xenon-containing structures. The pseudopotential basis set for Xe prevented the effective integration over the electron density, and we could not include the xenon species in the AIM analysis. In any

* To whom correspondence should be addressed. E-mail: fgrandi@unitus.it.

10.1021/jp102018n
Published on Web 06/18/2010

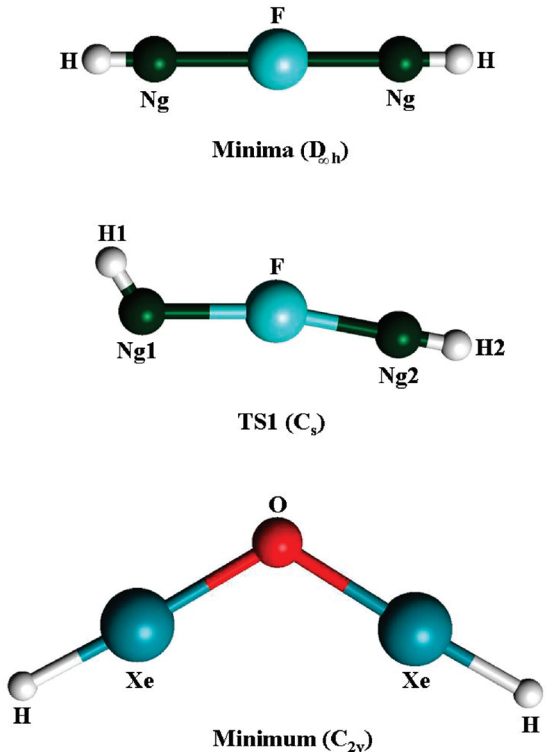

Figure 1. Connectivities of the $HNgFNgH^+$ energy minima and transition structures (Ng = He−Xe). The neutral HXeOXeH is also shown for comparison.

case, the results obtained for the lighter congeners are confidently sufficient to characterize the trends of the bonding properties of our investigated $HNgFNgH^+$.

3. Results and Discussion

3.1. Structure of $HNgFNgH^+$ (Ng = He−Xe). The connectivities of the presently investigated $HNgFNgH^+$ cations are shown in Figure 1, and their geometrical parameters are listed in Table 1.

At the MP2 level of theory, with both the aug-cc-pVDZ/SDD and the aug-cc-pVTZ/SDD basis sets, the linear species of $D_{\infty h}$ symmetry were characterized as energy minima. Their CCSD T1 diagnostics resulted well below the recommended threshold of 0.02,[49] thus suggesting that they should generally be well described by single-reference methods. To investigate the influence of correlation on the geometries, we recalculated the bond distances of any $HNgFNgH^+$ at the CCSD(T) level of theory. In addition, for the test-case $HHeFHeH^+$, we also calculated the CCSD(T)/aug-cc-pVDZ and CCSD(T)/aug-cc-pVTZ harmonic frequencies and confirmed its character of minimum-energy structure. The DFT-B3LYP method has been employed to investigate the structure and stability of experimentally observed noble-gas hydrides HNgY.[50] It has been particularly emphasized that, in certain situations, B3LYP may work better than MP2. We therefore also optimized the geometries of the $HNgFNgH^+$ cations at the B3LYP/aug-cc-pVTZ level of theory. Overall, the geometries of the linear $HNgFNgH^+$ revealed, however, only less sensitive to the theoretical level and to the basis set. At both the MP2 and CCSD(T) levels, the structures predicted with the aug-cc-pVTZ/SDD basis set are generally more compact, but the differences with the aug-cc-pVDZ/SDD bond distances amount to only 0.02−0.04 Å. In addition, for both the aug-cc-pVDZ/SDD and the aug-cc-pVTZ/SDD basis sets, the MP2 and CCSD(T) estimates are quite similar, with largest differences of only 0.007−0.008 Å for the bond distances of $HNeFNeH^+$. Finally, the MP2/aug-cc-pVTZ/SDD and B3LYP/aug-cc-pVTZ/SDD bond distances differ by only 0.02−0.03 Å, with a single larger difference of 0.054 Å for the H−Ne distance of $HNeFNeH^+$. The forthcoming discussion will be based on the CCSD(T)/aug-cc-pVTZ/SDD estimates.

The H−Ng bond distances of the $HNgFNgH^+$ cations periodically increase from $HHeFHeH^+$ to $HXeFXeH^+$ and are predicted as 0.749 (Ng = He), 0.977 (Ng = Ne), 1.281 (Ng = Ar), 1.424 (Ng = Kr), and 1.610 Å (Ng = Xe). The simplest comparable cationic species are the diatomic HNg^+, whose CCSD(T)/aug-cc-pVTZ/SDD bond distances are 0.776 (HHe^+), 0.992 (HNe^+), 1.282 (HAr^+), 1.416 (HKr^+), and 1.603 Å (HXe^+). Therefore, compared with HNg^+, the $HNgFNgH^+$ ions feature H−Ng bond distances that are only slightly longer for Kr and Xe, and even slightly shorter for Ar, and especially He and Ne. Overall, this suggests a tight hydrogen-noble gas interaction, and this is in line with the results of the AIM analysis (*vide infra*). The compactness of the $HNgFNgH^+$ cations is especially interesting for the helium and neon containing species. It confirms in fact that these two elements, usually reluctant to form neutral compounds, can be fixed into ionic fragments (especially cationic but also anionic) so as to form tightly bound species.[51−54] It is also of interest to note that the CCSD(T)/aug-cc-pVTZ/SDD H-Ng distances of the $HNgFNgH^+$ cations are quite similar to the H−Ng distances of the recently investigated $HNgCO^+$ cations[19] and follow, for any Ng, strictly analogous trends with respect to the diatomic HNg^+. The geometries of the linear $HNgFNgH^+$ can be also compared with the neutral HNgF. At the CCSD(T)/aug-cc-pVTZ/SDD level of theory, the H-Ng/Ng-F bond distances of these molecules are computed as 0.811 Å/1.415 Å (HHeF), 1.337 Å/1.992 Å (HArF), 1.477 Å/2.040 Å (HKrF), and 1.673 Å/2.129 Å (HXeF) (it is firmly established[20,24b] that, at the highest computational levels, HNeF is not a bound species). From Table 1, the Ng-F bond distances of $HNgFNgH^+$ are predicted as 1.594 (Ng = He), 2.085 (Ng = Ne), 2.193 (Ng = Ar), 2.250 (Ng = Kr), and 2.345 Å (Ng = Xe). Therefore, for any Ng, the H−Ng distance of HNgF is *longer* than $HNgFNgH^+$ by ca. 0.05 Å, and the Ng−F distance is *shorter* by ca. 0.18−0.22 Å. These qualitative structural differences are consistent with the predicted trends of the harmonic frequencies (*vide infra*).

The diatomic $H-Ng^+$ are covalent species,[55] and it is also known from previous studies[10,11] that, at their equilibrium geometries, the noble gas hydrides HNgY feature a covalent H−Ng bond and a strong ionic interaction, best described by the resonance form $(H-Ng^+)Y^-$.[10,11] The charge separation of $(H-Ng^+)F^-$ is particularly predicted to be as large as ca. +0.7 *e*/−0.7 *e*.[24b] Therefore, the strict geometric similarities with HNg^+ and HNgF suggest that the $HNgFNgH^+$ cations should be described as ion−dipole complexes between a fluoride anion F^- and two covalent H-Ng^+ cations, better formulated as $(H-Ng^+)_2F^-$. This structural assignment is confirmed by the NBO total charges and the AIM properties. The relevant MP2/aug-cc-pVTZ/SDD data are listed in Tables 2 and 3.

The negative charges of the F atoms range between −0.836 and −0.966 *e*, with the largest value for $HNeFNeH^+$. The HNg moieties also bear positive charges invariably larger than 0.9 *e*. The covalent and ionic character, respectively, of the H−Ng and Ng−F interactions is best supported by the AIM analysis. At the bcp of any H−Ng bond, the charge density is rather high, the corresponding Laplacian is negative, and the energy density has a negative value. Overall, these features point to shared-type, covalent interactions. On the other hand, at the bcp of any F−Ng bond, the charge density is low, the Laplacian is positive, and the energy density is essentially vanishingly small. These findings are typically related with closed-shell interactions, such as ionic, hydrogen, and

TABLE 1: Optimized Geometries (Å and °) of the $HNgFNgH^+$ Energy Minima and Transition Structures (Figure 1)

		min ($D_{\infty h}$)		**TS1** (C_s)						
species	method/basis set	H−Ng	Ng−F	H1−Ng1	H2−Ng2	Ng1−F	Ng2−F	H1−Ng1−F	H2−Ng2−F	Ng1−F−Ng2
$HHeFHeH^+$	MP2/aug-cc-pVDZ	0.751	1.615	0.750	0.750	1.723	1.605	120.7	179.8	169.4
	MP2/aug-cc-pVTZ	0.745	1.596	0.742	0.745	1.700	1.586	122.4	179.6	169.2
	B3LYP/aug-cc-pVTZ	0.777	1.576	0.768	0.780	1.700	1.566	115.1	178.8	165.6
	CCSD(T)/aug-cc-pVDZ	0.755	1.614	0.754	0.755	1.707	1.591	120.5	179.5	168.4
	CCSD(T)/aug-cc-pVTZ	0.749	1.594	0.745	0.749	1.694	1.584	122.3	179.4	168.8
$HNeFNeH^+$	MP2/aug-cc-pVDZ	0.996	2.088	0.996	0.996	2.114	2.087	148.4	179.7	175.2
	MP2/aug-cc-pVTZ	0.977	2.092	0.976	0.977	2.105	2.092	156.5	179.9	175.9
	B3LYP/aug-cc-pVTZ	1.031	2.073	1.013	1.036	2.122	2.068	137.6	179.6	171.9
	CCSD(T)/aug-cc-pVDZ	0.997	2.080							
	CCSD(T)/aug-cc-pVTZ	0.977	2.085							
$HArFArH^+$	MP2/aug-cc-pVDZ	1.293	2.225	1.280	1.297	2.468	2.184	108.2	180.0	174.2
	MP2/aug-cc-pVTZ	1.278	2.189	1.267	1.283	2.450	2.142	107.7	180.0	174.0
	B3LYP/aug-cc-pVTZ	1.305	2.189	1.281	1.318	2.468	2.135	105.7	180.0	172.7
	CCSD(T)/aug-cc-pVDZ	1.297	2.226							
	CCSD(T)/aug-cc-pVTZ	1.281	2.193							
$HKrFKrH^+$	MP2/aug-cc-pVDZ	1.432	2.276	1.414	1.440	2.598	2.209	102.7	180.0	175.5
	MP2/aug-cc-pVTZ	1.418	2.246	1.401	1.426	2.570	2.179	102.2	180.0	175.3
	B3LYP/aug-cc-pVTZ	1.449	2.257	1.422	1.466	2.600	2.187	101.2	180.0	175.1
	CCSD(T)/aug-cc-pVDZ	1.437	2.279							
	CCSD(T)/aug-cc-pVTZ	1.424	2.250							
$HXeFXeH^+$	MP2/aug-cc-pVDZ/SDD	1.615	2.364	1.591	1.629	2.765	2.273	98.4	180.0	177.4
	MP2/aug-cc-pVTZ/SDD	1.603	2.343	1.581	1.616	2.716	2.256	98.3	180.0	177.3
	B3LYP/aug-cc-pVTZ/SDD	1.633	2.370	1.601	1.651	2.758	2.284	98.2	180.0	176.6
	CCSD(T)/aug-cc-pVDZ/SDD	1.622	2.366							
	CCSD(T)/aug-cc-pVTZ/SDD	1.610	2.345							

TABLE 2: MP2/aug-cc-pVTZ/SDD NBO Atomic Charges q (e) of the $HNgFNgH^+$ Energy Minima and Transition Structures (Figure 1)

	min ($D_{\infty h}$)			**TS1** (C_s)				
species	H	Ng	F	H1	H2	Ng1	Ng2	F
$HHeFHeH^+$	0.596	0.322	−0.836	0.660	0.583	0.302	0.325	−0.870
$HNeFNeH^+$	0.727	0.256	−0.966	0.731	0.726	0.255	0.256	−0.968
$HArFArH^+$	0.382	0.549	−0.862	0.462	0.356	0.533	0.548	−0.899
$HKrFKrH^+$	0.266	0.654	−0.840	0.365	0.226	0.630	0.652	−0.873
$HXeFXeH^+$	0.117	0.803	−0.840	0.224	0.067	0.804	0.773	−0.868

TABLE 3: MP2/aug-cc-pVTZ AIM Analysis of the $HNgFNgH^+$ Energy Minima and Transition Structures (Ng = He, Ne, Ar, Kr) (Figure 1)[a]

		min ($D_{\infty h}$)		**TS1** (C_s)			
species	property	H−Ng	Ng−F	H1−Ng1	H2−Ng2	Ng1−F	Ng2−F
$HHeFHeH^+$	ρ	0.269	0.077	0.254	0.271	0.057	0.081
	$\nabla^2\rho$	−3.023	0.427	−3.546	−2.975	0.356	0.438
	H	−0.773	−0.001	−0.897	−0.762	0.006	−0.003
$HNeFNeH^+$	ρ	0.240	0.036	0.240	0.241	0.035	0.036
	$\nabla^2\rho$	−2.805	0.277	−2.893	−2.806	0.269	0.277
	H	−0.752	0.012	−0.773	−0.752	0.012	0.012
$HArFArH^+$	ρ	0.244	0.055	0.241	0.244	0.031	0.063
	$\nabla^2\rho$	−1.023	0.255	−1.234	−0.963	0.160	0.278
	H	−0.308	−0.001	−0.353	−0.295	0.004	−0.003
$HKrFKrH^+$	ρ	0.213	0.057	0.214	0.211	0.029	0.069
	$\nabla^2\rho$	−0.618	0.231	−0.703	−0.582	0.135	0.253
	H	−0.205	−0.003	−0.306	−0.221	0.003	−0.003

[a] The charge density ρ ($e\ a_0^{-3}$), the Laplacian of the charge density $\nabla^2\rho$ ($e\ a_0^{-5}$), and the energy density H (hartree a_0^{-3}) are calculated at the bcp on the specified bond.

van der Waals bonds. It is also of interest to compare the charges of the H and Ng atoms of the $HNgFNgH^+$ cations with the atomic charges of the diatomic HNg^+. At the MP2/aug-cc-pVTZ/SDD level of theory, the H/Ng NBO charges of the HNg^+ cations are 0.741 e/0.259 e (HHe^+), 0.778 e/0.222 e (HNe^+), 0.497 e/0.503 e (HAr^+), 0.393 e/0.607 e (HKr^+), and 0.250 e/0.750 e (HXe^+). Therefore, while the electrostatic interaction with F^- essentially does not alter the total group charge of the HNg^+ cations, it still induces an appreciable charge shift from the noble gas to the hydrogen atom. Interestingly, similar to the $HNgFNgH^+$, the $HNgCO^+$ cations were structurally assigned as ion−dipole complexes between a covalent HNg^+ and CO.[19]

3.2. Harmonic Vibrational Frequencies. The MP2 harmonic frequencies and IR intensities of the $HNgFNgH^+$ energy minima are listed in Table 4. The results are generally only little affected by the basis set, and we will refer in particular to the MP2/aug-cc-pVTZ/SDD estimates.[56]

The 10 molecular vibrations expected for a linear $HNgFNgH^+$ of $D_{\infty h}$ symmetry are grouped into two H−Ng stretchings (symmetric and asymmetric), two Ng−F stretchings (symmetric and asymmetric), two doubly degenerate H−Ng−F bendings (π_g and π_u), and one doubly degenerate Ng−F−Ng bending (π_u). Within each symmetry, the various motions resulted essentially uncoupled, and it was possible to unequivocally recognize all the expected molecular vibrations. Consistent with the covalent character of the H−Ng bonds, the corresponding stretching frequencies are particularly high. The wave numbers of the symmetric and asymmetric components are quite close (they become nearly degenerate for the heaviest members of the series), and the IR-active asymmetric modes are particularly predicted at 3637 (Ng = He), 3113 (Ng = Ne), 2754 (Ng = Ar), 2550 (Ng = Kr), and 2288 cm^{-1} (Ng = Xe). For comparison, at the MP2/aug-cc-pVTZ/SDD level of theory, the harmonic frequencies of the diatomic HNg^+ are 3212 (HHe^+), 2916 (HNe^+), 2738 (HAr^+), 2576 (HKr^+), and 2333 (HXe^+), and the H−Ng stretching frequencies of HNgF are 2715 (Ng = He), 2303 (Ng = Ar), 2223 (Ng = Kr), and 2063 cm^{-1} (Ng = Xe). The predicted differences of these harmonic frequencies nicely reflect the trends of the various H−Ng bond distances. Thus, the shorter H−Ng distances of $HNgFNgH^+$ with respect to HNgF and the shorter H−He and H−Ne distance of $HHeFHeH^+$ and $HNeFNeH^+$ with respect to HHe^+ and HNe^+, respectively, are invariably associated with higher harmonic frequencies. On the other hand, the lower H−Ng frequencies of $HKrFKrH^+$ and $HXeFXeH^+$ with respect to HKr^+ and HXe^+ parallel the longer bond distances of the $HNgFNgH^+$. In any case, compared with HNg^+ and HNgF, the H−Ng asymmetric stretching of any $HNgFNgH^+$ is generally weaker by 1 or 2 orders of magnitude. Unlike the H−Ng stretching motions, the symmetric and asymmetric Ng−F stretching motions of $HNgFNgH^+$ occur at clearly

TABLE 4: Harmonic Vibrational Frequencies (cm^{-1}) of the Linear ($D_{\infty h}$) $HNgFNgH^+$[a]

		assignment						
species	method/basis set	ν_s(H−Ng)[b]	ν_{as}(H−Ng)[c]	ν_s(Ng−F)[b]	ν_{as}(Ng−F)[c]	δ(H−Ng−F)[d]	δ(H−Ng−F)[e]	δ(Ng−F−Ng)[e]
$HHeFHeH^+$	MP2/aug-cc-pVDZ	3613 (0)	3651 (65)	660 (0)	699 (1081)	611 (0)	613 (246)	168 (384)
	MP2/aug-cc-pVTZ	3600 (0)	3637 (62)	677 (0)	718 (1089)	531 (0)	527 (271)	146 (346)
$HNeFNeH^+$	MP2/aug-cc-pVDZ	2798 (0)	2817 (386)	263 (0)	445 (234)	350 (0)	315 (579)	94 (147)
	MP2/aug-cc-pVTZ	3100 (0)	3113 (475)	261 (0)	442 (215)	166 (0)	188 (643)	83 (69)
$HArFArH^+$	MP2/aug-cc-pVDZ	2719 (0)	2726 (48)	201 (0)	403 (394)	515 (0)	517 (154)	81 (82)
	MP2/aug-cc-pVTZ	2748 (0)	2754 (57)	205 (0)	404 (422)	534 (0)	535 (143)	78 (76)
$HKrFKrH^+$	MP2/aug-cc-pVDZ	2530 (0)	2532 (3)	144 (0)	377 (438)	525 (0)	526 (81)	77 (47)
	MP2/aug-cc-pVTZ	2549 (0)	2550 (5)	149 (0)	389 (452)	533 (0)	534 (75)	70 (43)
$HXeFXeH^+$	MP2/aug-cc-pVDZ/SDD	2285 (0)	2283 (6)	118 (0)	365 (499)	481 (0)	484 (21)	68 (27)
	MP2/aug-cc-pVTZ/SDD	2290 (0)	2288 (7)	120 (0)	370 (502)	490 (0)	494 (18)	73 (25)

[a] IR intensities (km mol^{-1}) are given in parentheses. [b] Symmetric stretching. [c] Asymmetric stretching. [d] Doubly degenerate bending (π_g). [e] Doubly degenerate bending (π_u).

distinguishable wave numbers, with a largest difference of ca. 250 cm^{-1} for $HKrFKrH^+$ and $HXeFXeH^+$. For any $HNgFNgH^+$, the higher wavenumber is invariably associated with the IR-active asymmetric mode, predicted at 718 (Ng = He), 442 (Ng = Ne), 404 (Ng = Ar), 389 (Ng = Kr), and 370 cm^{-1} (Ng = Xe). Consistent with the invariably shorter F−Ng bond distances of the neutral HNgF, at the MP2/aug-cc-pVTZ/SDD level of theory, the Ng−F stretching frequencies of these molecules are computed as 1020 (Ng = He), 477 (Ng = Ar), 458 (Ng = Kr), and 452 cm^{-1} (Ng = Xe). Not unexpectedly, the two H-Ng-F bending motions of π_g and π_u symmetry of the $HNgFNgH^+$ are nearly degenerate, and predicted between 490 and 530 cm^{-1}. The H−Ne−F bending motions of $HNeFNeH^+$ occur instead at lowest wave numbers of less than 200 cm^{-1}. The MP2/aug-cc-pVTZ/SDD bending motions of the HNgF are invariably comparably higher and predicted in particular at 811 (Ng = He), 742 (Ng = Ar), 713 (Ng = Kr), and 638 cm^{-1} (Ng = Xe). Finally, for any $HNgFNgH^+$, the two degenerate Ng−F−Ng bending motions occur at the lowest wave numbers, usually predicted at less than 100 cm^{-1}.

3.3. Dissociation Energies and Stabilities. The stability of the $HNgFNgH^+$ cations depends on the energetics and the activation barriers of their dissociation channels. The conceivable processes of lowest energy include in particular the following reactions:

$$HNgFNgH^+ \rightarrow HNg^+ + HNgF \quad (1)$$

$$HNgFNgH^+ \rightarrow HNg^+ + H + Ng + F \quad (2)$$

$$HNgFNgH^+ \rightarrow 2HNg^+ + F^- \quad (3)$$

$$HNgFNgH^+ \rightarrow HNg^+ + Ng + HF \quad (4)$$

$$HNgFNgH^+ \rightarrow HF^+ + H + 2Ng \quad (5)$$

$$HNgFNgH^+ \rightarrow H_2F^+ + 2Ng \quad (6)$$

We calculated the energy changes at 0 K (ΔE) of reactions 1−6, and the activation barriers $E^{\ddagger}$ of the elementary steps conceivably involved in the exothermic reactions 4, 5, and 6 at the B3LYP/aug-cc-pVTZ/SDD, MP2/aug-cc-pVTZ/SDD, and CCSD(T)/aug-cc-pVTZ/SDD//MP2/aug-cc-pVTZ/SDD levels of theory. The results obtained are collected in Table 5.

At the B3LYP level of theory, the ΔE of reaction 1 is comparable with that of MP2, while the ΔEs of reactions 2−6 are larger than that of MP2 by 5−12 kcal mol^{-1}. However, the activation barriers predicted by the two methods differ by less than 1 or 2 kcal mol^{-1}. Therefore, even though the B3LYP method predicts a thermochemical stability of the $HNgFNgH^+$ cations slightly larger than MP2, the two methods predict a quite comparable kinetic stability. The MP2 and the CCSD(T) estimates are also quite similar, and differ typically by less than 1 or 2 kcal mol^{-1}. The only exceptions are the ΔE of reactions 2 and 5, which are overestimated by ca. 3−5 kcal mol^{-1} at the MP2 level of theory. This finding is, however, not unexpected. It is in fact known from a previous study[29c] that, compared with the CCSD(T), the MP2 method systematically overestimates the atomization energies of the neutral XNgY. In particular, with the aug-cc-pVTZ basis set, the atomization energy of HArF is computed (with no ZPE) as 9.7 kcal mol^{-1} at the MP2 level of theory and 5.4 kcal mol^{-1} at the CCSD(T) level of theory.[29c] The forthcoming discussion will be based on the CCSD(T)/aug-cc-pVTZ/SDD//MP2/aug-cc-pVTZ/SDD estimates.[57]

For any Ng, reaction 1 is definitely endothermic. The values of $\Delta E(1)$ range in fact between 46.2 (Ng = He) and 40.3 kcal mol^{-1} (Ng = Xe), and these large interaction energies reflect the large dipole moments and polarizabilites of the HNgF molecules.[25a] As a matter of fact, with the only exception of $HNeFNeH^+$, the interaction between HNg^+ and HNgF is indeed so large that, despite the intrinsic instability or only marginal stability of HHeF and HArF with respect to the three-body dissociation,[29c] the four-body dissociation (2) of $HHeFHeH^+$ and $HArFArH^+$ is endothermic by 20.1 and 40.6 kcal mol^{-1}, respectively. This finding is in line with our recent study,[59] which shows that the complexation energies of HHeF with strong electrophilic species such as alkali metal cations and molecules are large enough to inhibit the dissociation of HHeF into H + He + F. For $HKrFKrH^+$ and $HXeFXeH^+$, reaction 2 is endothermic by 58.8 and 79.2 kcal mol^{-1}, respectively. The ΔEs of reaction 3 are also exceedingly positive, and this reflects the strongly endothermic character of the heterolytic dissociation of any HNgF into $HNg^+ + F^-$.[20] For any $HNgFNgH^+$, reactions 4 and 6 are instead largely exothermic, and reaction 5 is also exothermic for both $HHeFHeH^+$ and $HNeFNeH^+$. All the $HNgFNgH^+$ cations can therefore exist only as metastable species, and we investigated the activation barriers of their exothermic dissociations. The decomposition of any $HNgFNgH^+$ commences through the planar transition structures **TS1** shown in Figure 1. Their geometries, charge distributions, and AIM properties are collected in Tables 1, 2, and 3. These species were located at the MP2 level of theory with both the aug-cc-pVDZ/SDD and aug-cc-pVTZ/SDD basis sets,[60] and their CCSD T1 diagnostics resulted well below the recommended threshold

TABLE 5: Dissociation Energies at 0 K (kcal mol^{-1}) of the HNgFNgH$^+$ Cations (Reference Species) Calculated with the aug-cc-pVTZ/SDD Basis Set[a]

species	method	$HNg^+ + HNgF$[b]	$HNg^+ + H + Ng + F$	$2HNg^+ + F^-$	$HNg^+ + Ng + HF$	$HF^+ + H + 2Ng$	$H_2F^+ + 2Ng$	$E^{\ddagger}$[c]
$HHeFHeH^+$	MP2	46.3 (46.9)	25.1 (26.2)	213.1 (214.2)	−111.6	−10.7	−184.2	0.8
	B3LYP	47.1 (47.2)	33.5 (33.5)	225.3 (225.5)	−99.8	−2.6	−172.6	2.4
	CCSD(T)[d]	46.2 (46.7)	20.1 (21.2)	215.0 (216.1)	−112.2	−16.0	−185.2	0.7/0.8[e]
$HNeFNeH^+$	MP2		−8.8 (−9.0)	171.1 (172.0)	−146.8	−39.0	−212.5	−0.3
	B3LYP	37.6 (37.7)	−3.3 (−3.3)	181.9 (182.1)	−136.5	−32.6	−202.6	0.3
	CCSD(T)[d]		−12.2 (−14.3)	172.8 (173.7)	−147.7	−44.6	−213.8	−0.1
$HArFArH^+$	MP2	44.0 (44.6)	45.5 (48.2)	187.6 (188.0)	−89.6	58.7	−114.8	8.5
	B3LYP	42.3 (42.4)	49.3 (49.3)	193.3 (193.5)	−84.0	61.0	−108.9	10.0
	CCSD(T)[d]	43.6 (44.2)	40.6 (43.4)	188.6 (189.8)	−90.0	54.7	−114.5	9.7
$HKrFKrH^+$	MP2	42.5 (43.9)	63.3 (69.0)	193.6 (196.1)	−68.8	92.9	−80.6	12.1
	B3LYP	41.6 (41.7)	67.0 (67.1)	198.2 (198.4)	−66.2	91.7	−78.3	13.1
	CCSD(T)[d]	41.3 (43.6)	58.8 (64.5)	194.4 (197.1)	−68.9	89.7	−79.5	12.0
$HXeFXeH^+$	MP2	40.7 (41.9)	83.2 (88.1)	197.5 (199.6)	−49.7	127.6	−45.9	14.8
	B3LYP	40.0 (40.0)	84.2 (84.3)	199.9 (200.2)	−49.0	124.4	−45.6	15.3
	CCSD(T)[d]	40.3 (41.6)	79.2 (84.4)	198.5 (200.8)	−48.8	126.1	−43.1	14.8

[a] The values in parentheses do not include the BSSE. [b] At the MP2 level of theory, HNeF is not an energy minimum. [c] Energy barrier for the eventual decomposition of $HNgFNgH^+$ (see text). [d] At the MP2/aug-cc-pVTZ/SDD optimized geometries. [e] At the CCSD(T)/aug-cc-pVTZ/SDD optimized geometry.

of 0.02. We also confirmed the **TS1** at the B3LYP/aug-cc-pVTZ/SDD level of thery. As shown in Table 1, likewise the energy minima, the B3LYP/aug-cc-pVTZ/SDD, and the MP2/aug-cc-pVTZ/SDD optimized parameters of **TS1** differ by only 0.02−0.04 Å in the bond lengths, and by 1−7° degrees in the bond angles. We notice a single larger difference of ca. 19° in the H1−Ne1−F bond angle of the neon-containing structure. For $HHeFHeH^+$, the existence of **TS1** was also confirmed at the CCSD(T)/aug-cc-pVDZ and CCSD(T)/aug-cc-pVTZ levels of theory. Passing from any minimum to the corresponding **TS1**, the H1−Ng1−F bond angle closes by nearly 60° in $HHeFHeH^+$ up to nearly 80° in $HXeFXeH^+$. The Ng1−F bond distance is also appreciably longer than the linear $HNgFNgH^+$, and the H2−Ng2 and Ng2−F bond distances are only slightly longer and shorter, respectively. Consistent with these asymmetric structural changes, passing from any $HNgFNgH^+$ minimum to the corresponding **TS1**, the most important variations of charge distribution and AIM properties involve the H1 and Ng1 atoms and the H1−Ng1 and Ng1−F bond (see Tables 2 and 3). At the CCSD(T)/aug-cc-pVTZ/SDD//MP2/aug-cc-pVTZ/SDD level of theory and 0 K, the energy differences between the various $HNgFNgH^+$ energy minima and the corresponding **TS1** are computed as 0.7 kcal mol^{-1} for $HHeFHeH^+$ (a nearly coincident value of 0.8 kcal mol^{-1} is obtained at the CCSD(T)/aug-cc-pVTZ level of theory), nearly zero for $HNeFNeH^+$, and 9.7, 12.0, and to 14.8 kcal mol^{-1}, respectively, for $HArFArH^+$, $HKrFKrH^+$, and $HXeFXeH^+$. The B3LYP/aug-cc-pVTZ estimates are quite similar. The neutral HNgF eliminate HF by bent transition structures,[10,11] and we therefore initially regarded **TS1** as the transition structures for reactions 4. However, the IRC calculations performed at the MP2/aug-cc-pVTZ/SDD level of theory confirmed this expectation only for $HXeFXeH^+$. For the other congeners, **TS1** was ascertained to be the transition structure for the eventual extrusion of two Ng atoms and the formation of H_2F^+ (despite careful searching, we could not locate, neither at the B3LYP nor at the MP2 level of theory, the conceivable transition structure for reaction 6 with both the H−Ng−F bond angles flattened to less than 180° and the two H atoms in cis conformation to each other). For the lightest $HHeFHeH^+$ and $HNeFNeH^+$, using **TS1** as the starting point, the IRC calculations yield directly two He or Ne atoms and H_2F^+. For the heaviest $HArFArH^+$, $HKrFKrH^+$, and $HXeFXeH^+$, they yield instead Ng···$HNgFH^+$ complexes, which are nearly degenerate with separated Ng and $HNgFH^+$ (Ng = Ar, Kr, Xe). We investigated the subsequent fate of the $HNgFH^+$ intermediates, and the relevant data are reported in Figure 2.

The linear $HNgFH^+$ are true energy minima on the MP2/aug-cc-pVTZ potential energy surface. The long Ng−F bond distances and the NBO atomic charges point to ion−dipole complexes between HNg^+ and HF. This is in line with the AIM analysis, which confirmed the covalent character of the H−Ng and H−F bonds, and the ionic character of the Ng−F interaction. At the CCSD(T)/aug-cc-pVTZ/SDD//MP2/aug-cc-pVTZ/SDD

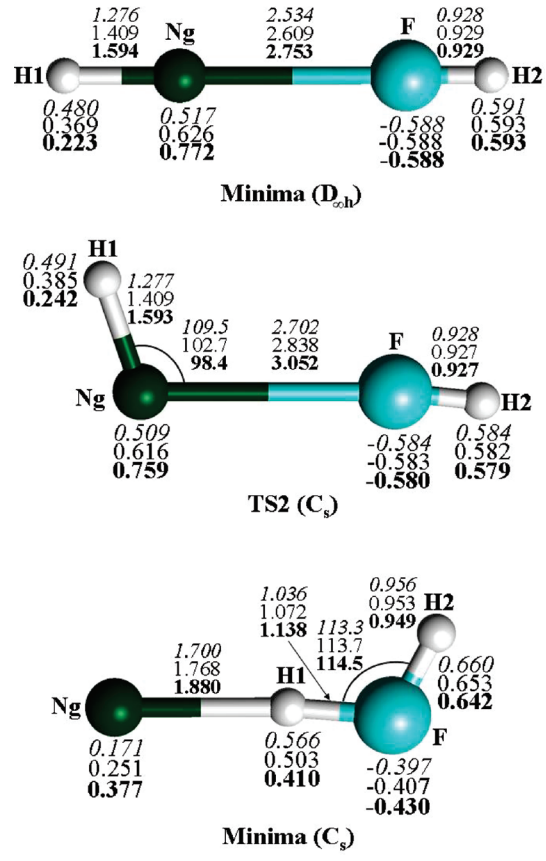

Figure 2. MP2/aug-cc-pVTZ/SDD optimized geometries (Å and degrees) and NBO atomic charges (e) of the $HNgFH^+$ and Ng−H_2F^+ ions involved in the decomposition of $HNgFNgH^+$ (Ng = Ar, Kr, Xe). Italics, normal, and bold values refer to Ar, Kr, and Xe, respectively.

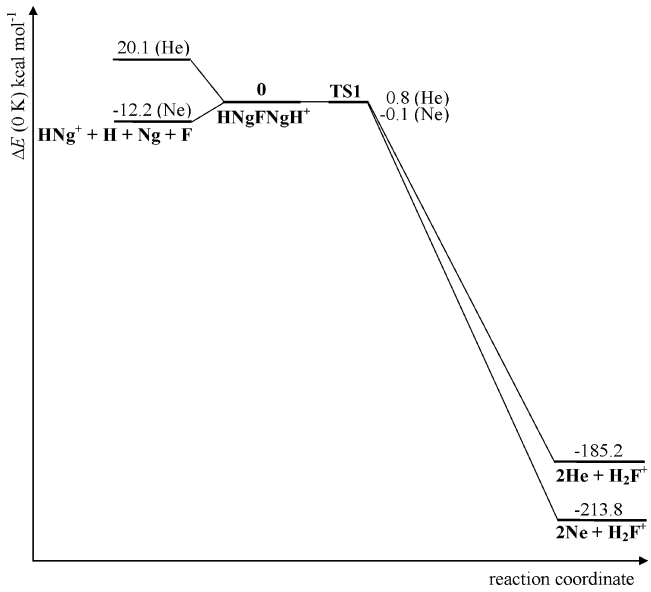

Figure 3. Decomposition paths of $HHeFHeH^+$ and $HNeFNeH^+$ calculated at the CCSD(T)/aug-cc-pVTZ/SDD//MP2/aug-cc-pVTZ/SDD level of theory and 0 K.

level of theory and 0 K, the complexation energies between HNg^+ and HF are 9.9 kcal mol^{-1} for Ng = Ar, and 10.1 kcal mol^{-1} for Ng = Kr and Xe. The linear $HNgFH^+$ can exothermically isomerize into $Ng\cdots H_2F^+$ complexes passing through the bent transition structures **TS2**.[61] This requires the closening of the H1−Ng−F bond angle, which reduces by nearly 70−80°, and the activation barriers are predicted as 1.1 kcal mol^{-1} for Ng = Ar, 2.1 kcal mol^{-1} for Ng = Kr, and 2.8 kcal mol^{-1} for Ng = Xe. The $Ng\cdots H_2F^+$ cations may in turn decompose into HNg^+ + HF or Ng + H_2F^+. Consistent with the proton affinities (PAs)[58] of HF (115.7 kcal mol^{-1}), Ar (88.2 kcal mol^{-1}), Kr (101.5 kcal mol^{-1}), and Xe (119.4 kcal mol^{-1}), our calculations predict that the decomposition of lower energy of both $Ar-H_2F^+$ and $Kr-H_2F^+$ is the loss of the noble gas and the formation H_2F^+, while $Xe\cdots H_2F^+$ preferentially decomposes into HXe^+ and HF.

Overall, our calculations support the following decomposition paths of the $HNgFNgH^+$ cations. The lightest $HHeFHeH^+$ and $HNeFNeH^+$ directly decompose into two Ng atoms and H_2F^+ passing through **TS1**. As shown in Figure 3, the involved activation barriers are negligibly small, and the ions are predicted to be essentially unstable. The heaviest $HArFArH^+$, $HKrFKrH^+$, and $HXeFXeH^+$ decompose instead by the three-step sequences diagrammatically shown in Figure 4.

All the ions first pass through **TS1** and extrude an Ng atom, so as to form the linear $HNgFH^+$. These intermediates undergo the exothermic isomerization into $Ng\cdots H_2F^+$, which in turn dissociates into Ng and H_2F^+ for Ng = Ar and Kr, and into HXe^+ and HF for Ng = Xe. Thus, the $HNgFNgH^+$ cations offer an intriguing example of different decomposition paths (xenon vs lightest congeners) of structurally similar noble gas compounds. In any case, for $HArFArH^+$, $HKrFKrH^+$, and $HXeFXeH^+$, the rate-determining barriers corresponding to **TS1** are invariably large enough to support their conceivable existence as metastable species.

Likewise other series of noble-gas neutrals and ions, including HNgF,[20] the neon-containing structure is the least stable among the various $HNgFNgH^+$ isomers. Inspection of Tables 2 and 4 reveal in particular large qualitative differences in the behavior of $HNeFNeH^+$ with respect to the other congeners. First, all values of charges on H, Ng, and F predicted for Ne do not fit into the monotonic progression of properties from He to Xe. Second, the predicted properties of $HNeFNeH^+$ are the most sensitive to the computational method used within the entire $HNgFNgH^+$ family. For example, the calculated frequencies of the symmetric and asymmetric Ne−H stretching modes differ by as much as 300 cm^{-1} for the aug-cc-pVDZ and the aug-cc-pVTZ basis set. This anomalous behavior of Ne has been already noticed before[62−64] and is usually ascribed to the presence (in contrast with He) of its repulsive valence *p* orbitals.

3.4. Comparison between HNgF and $HNgFNgH^+$ (Ng = He, Ar, Kr, Xe). The $HNgFNgH^+$ cations are the simplest ionic counterparts of the neutral HNgF. We in fact optimized the geometries of the $HNgF^+$ cations but invariably experienced their unstability with respect to HNg^+ and F. The properties of HNgF and $HNgFNgH^+$ are systematically compared in Table 6 (we excluded from the discussion the intrinsically unstable HNeF).

The charge distributions and the AIM properties of both HNgF and $HNgFNgH^+$ indicate that these species must be similarly viewed as ion−dipole complexes between a fluoride anion and one or two covalent $H-Ng^+$ cations, best described as $(H-Ng^+)F^-$and $(H-Ng^+)_2F^-$, respectively. Compared with HNgF, the $HNgFNgH^+$ feature a charge flux of nearly 0.10−0.20 *e* from the fluorine to the hydrogen atoms and a consequent more pronounced ion-pair character. Interestingly, the positive charges of the noble gas atoms are only slightly different. Passing from any HNgF to the corresponding $HNgFNgH^+$, the H−Ng bond length decreases and the Ng−F bond length increases. The shortening of the H−Ng distances ranges around 0.04−0.05 Å, while the lengthening of the Ng−F distance is in general more pronounced and predicted as ca. 0.15−0.20 Å. These structural changes are invariably accompanied by consistent changes of the harmonic frequencies, namely a blue shift (increase of the harmonic frequency and decrease of the IR intensity) of the H−Ng stretching mode, and a red shift (decrease of the harmonic frequency and increase of the IR intensity) of the Ng−F stretching mode. The H−Ng−F bending mode is also invariably red-shifted. The effects are particularly pronounced for the helium species, and decrease in the periodic order from helium to xenon.

As for the stability of HNgF and $HNgFNgH^+$, the cationic species are in general thermochemically more stable than their neutral analogues. We note in particular that the dissociations of HHeF and HArF into H + Ng + F (Ng = He, Ar) are exothermic or thermoneutral, but the dissociations of $HNgFNgH^+$ into HNg^+ + H + Ng + F (Ng = He, Ar) are definitely endothermic. However, compared with the neutral HNgF, the $HNgFNgH^+$ cations feature lower *kinetic* stability. The decomposition barriers are in fact invariably lower, and are predicted in particular as negligibly small for the helium cation $HHeFHeH^+$. Therefore, in line with the conclusions from our recent study on the conceivable stabilization of HHeF by complexation,[59] the present results confirm that cationic species can in principle stabilize the HNgF molecules with respect to the three-body dissociation but drastically reduce their bending barriers.

3.5. Comparison between $HXeFXeH^+$ and HXeOXeH. The xenon cation $HXeFXeH^+$ is isoelectronic with the experimentally observed HXeOXeH,[15] and it is therefore of interest to compare the structure and properties of these two species. While the cation is linear, the neutral species is bent, with a Xe−O−Xe bond angle computed as 124.5° at the MP2 level of theory with a triple-ζ quality basis set. As for the bond distances, the Xe−F bond of $HXeFXeH^+$ is longer than the

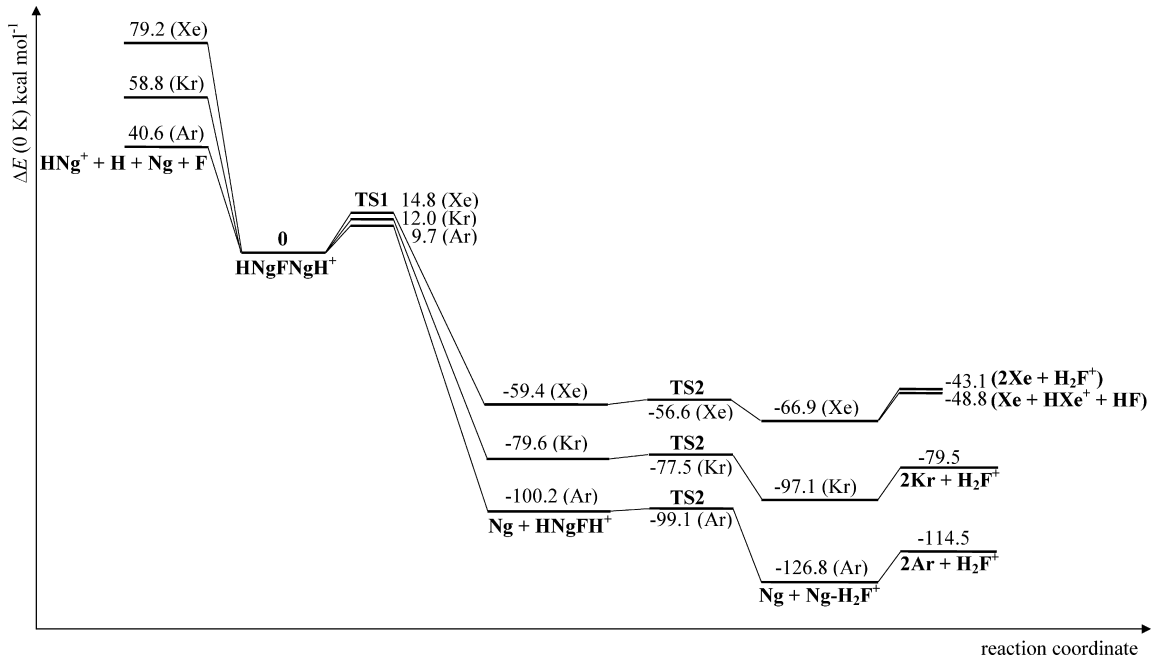

Figure 4. Decomposition paths of $HNgFNgH^+$ (Ng = Ar, Kr, Xe) calculated at the CCSD(T)/aug-cc-pVTZ/SDD//MP2/aug-cc-pVTZ/SDD level of theory and 0 K.

TABLE 6: Properties of the Linear HNgF and $HNgFNgH^+$ (Ng = He, Ar, Kr, Xe) at the MP2/aug-cc-pVTZ/SDD Level of Theory[a]

	HHeF	$HHeFHeH^+$	HArF	$HArFArH^+$	HKrF	$HKrFKrH^+$	HXeF	$HXeFXeH^+$
R(H-Ng)	0.790	0.745	1.319	1.278	1.461	1.418	1.656	1.603
R(Ng-F)	1.409	1.596	1.982	2.189	2.035	2.246	2.130	2.343
ν(H-Ng)[b]	2715 (2475)	3600 (0)[c] 3637 (62)[d]	2303 (899)	2748 (0)[c] 2754 (57)[d]	2223 (534)	2549 (0)[c] 2550 (5)[d]	2063 (368)	2290 (0)[c] 2288 (7)[d]
ν(Ng-F)[b]	1020 (520)	677 (0)[c] 718 (1089)[d]	477 (265)	205 (0)[c] 404 (422)[d]	458 (210)	149 (0)[c] 389 (452)[d]	452 (193)	120 (0)[c] 370 (502)[d]
δ(H-Ng-F)[e]	811 (37)	531 (0)[f] 527 (271)[g]	742 (30)	534 (0)[f] 535 (143)[g]	713 (9)	533 (0)[f] 534 (75)[g]	638 (0.2)	490 (0)[f] 494 (18)[g]
q(H)[h]	0.358	0.596	0.228	0.382	0.106	0.263	−0.042	0.117
q(Ng)[h]	0.326	0.322	0.534	0.549	0.648	0.654	0.813	0.803
q(F)[h]	−0.685	−0.835	−0.763	−0.862	−0.754	−0.840	−0.771	−0.840
ρ(H-Ng)[i]	0.271	0.269	0.228	0.244	0.197	0.213		
$\nabla^2\rho$(H-Ng)[j]	−1.985	−3.023	−0.668	−1.023	−0.454	−0.618		
H(H-Ng)[k]	−0.542	−0.773	−0.230	−0.308	−0.172	−0.205		
ρ(Ng-F)[i]	0.144	0.077	0.098	0.055	0.100	0.057		
$\nabla^2\rho$(Ng-F)[j]	0.568	0.427	0.337	0.255	0.279	0.231		
H(Ng-F)[k]	−0.045	−0.001	−0.022	−0.001	−0.030	−0.003		
ΔE [H + Ng + F (+ HNg^+)][l]	−24.7	20.1	1.30	40.6	16.4	58.8	38.3	79.2
$E^{\neq m}$	6.5	0.7	22.3	9.7	30.6	12.0	37.0	14.8

[a] The energy changes and energy barriers are calculated by CCSD(T)/aug-cc-pVTZ/SDD//MP2/aug-cc-pVTZ/SDD single-point calculations. [b] Stretching harmonic frequency (cm^{-1}). IR intensity (km mol^{-1}) in parentheses. [c] Symmetric component. [d] Asymmetric component. [e] Doubly degenerate bending harmonic frequency (cm^{-1}). IR intensity (km mol^{-1}) in parentheses. [f] π_g component. [g] π_u component. [h] NBO total charge (e). [i] Charge density ($e\ a_0^{-3}$) at the bcp on the specified bond. [j] Laplacian of the charge density ($e\ a_0^{-5}$) at the bcp on the specified bond. [k] Energy density (hartree a_0^{-3}) at the bcp on the specified bond. [l] Energy change at 0 K (kcal mol^{-1}) of the dissociation $HNgF(NgH^+) \rightarrow H + Ng + F (+ HNg^+)$ (including the BSSE). [m] Energy barrier for the elimination of HF from HNgF and for the eventual decomposition of $HNgFNgH^+$ (see text).

Xe−O bond of HXeOXeH by nearly 0.2 Å, but the H−Xe bond is shorter by 0.15 Å. Consistently, the harmonic frequency of the asymmetric H−Xe stretching band, presently computed at 2288 cm^{-1} for $HXeFXeH^+$, is predicted at 1572 cm^{-1} for HXeOXeH (the experimental value is 1380 cm^{-1}). As for the stability of $HXeFXeH^+$ and HXeOXeH, the MP2 bending barrier for the decomposition of HXeOXeH into HXeOH + Xe, computed as 0.57 eV (13.1 kcal mol^{-1}),[16] is very close to our predicted MP2 barrier of 14.8 kcal mol^{-1} for the decomposition of $HXeFXeH^+$ into $HXeFH^+$ + Xe. However, while HXeOXeH is protected by a barrier of 0.4 eV (9.2 kcal mol^{-1}) with respect to dissociation into HXeO + Xe + H,[16] $HXeFXeH^+$ is much more stable with respect to dissociation into HXe^+ + H + Xe + F (by at least ca. 80 kcal mol^{-1}), and into HXe^+ + HXeF (by at least ca. 40 kcal mol^{-1}). Therefore, the cationic species appears more compact overall than its neutral analogue.

4. Concluding Remarks

The presently investigated $HNgFNgH^+$ are exemplary cases of cationic noble gas hydrides containing two Ng atoms. The helium and neon species are essentially unstable, but the heaviest congeners $HArFArH^+$, $HKrFKrH^+$, and $HXeFXeH^+$ are predicted to be metastable with respect to decomposition into HNg^+ + Ng + HF or H_2F^+ + 2Ng. These findings suggest the intriguing prospect that, under proper conditions, the $HXeFXeH^+$ cation, and probably also $HArFArH^+$ and $HKrFKrH^+$, could be actually experimentally observed. If prepared, these species would rank among very few examples of entities containing two noble gas

atoms. We hope that our calculations could stimulate future experimental work in this direction.

Acknowledgment. The authors thank the Università della Tuscia and the Italian Ministero dell'Università e della Ricerca (MiUR) for financial support through the "Cofinanziamento di Programmi di Ricerca di Rilevante Interesse Nazionale".

References and Notes

(1) Pettersson, M.; Lundell, J.; Räsänen, M. *Eur. J. Inorg. Chem.* **1999**, 729–737.
(2) Seidel, S.; Seppelt, K. *Science* **2000**, *290*, 117–118.
(3) Pyykkö, P. *Science* **2000**, *290*, 64–65.
(4) Christe, K. O. *Angew. Chem., Int. Ed.* **2001**, *40*, 1419–1421.
(5) Li, J.; Bursten, B. E.; Liang, B.; Andrews, L. *Science* **2002**, *295*, 2242–2245.
(6) Grochala, W. *Chem. Soc. Rev.* **2007**, *36*, 1632–1655.
(7) Muck, L. A.; Timoshkin, A. Y.; v. Hopffgarten, M.; Frenking, G. *J. Am. Chem. Soc.* **2009**, *131*, 3942–3949.
(8) (a) Roithová, J.; Schröder, D. *Angew. Chem., Int. Ed.* **2009**, *48*, 8788–8790. (b) Lockyear, J. F.; Douglas, K.; Price, S. D.; Karkowska, M.; Fijalkowski, K. J.; Grochala, W.; Remeš, M.; Roithová, J.; Schröder, D. *J. Phys. Chem. Lett.* **2010**, *1*, 358–362.
(9) Justik, M. W. *Annu. Rep. Prog. Chem., Sect. A* **2009**, *105*, 165–176.
(10) Gerber, R. B. *Annu. Rev. Phys. Chem.* **2004**, *55*, 55–78.
(11) Khriachtchev, L.; Räsänen, M.; Gerber, R. B. *Acc. Chem. Res.* **2009**, *42*, 183–191, and references therein.
(12) Khriachtchev, L.; Pettersson, M.; Runeberg, N.; Lundell, J.; Räsänen, M. *Nature* **2000**, *406*, 874–876.
(13) Frenking, G. *Nature* **2000**, *406*, 836–837.
(14) Khriachtchev, L.; Tanskanen, H.; Lundell, J.; Pettersson, M.; Kiljunen, H.; Räsänen, M. *J. Am. Chem. Soc.* **2003**, *125*, 4696–4697.
(15) Khriachtchev, L.; Isokoski, K.; Cohen, A.; Räsänen, M.; Gerber, R. B. *J. Am. Chem. Soc.* **2008**, *130*, 6114–6118.
(16) Tsivion, E.; Gerber, R. B. *Chem. Phys. Lett.* **2009**, *482*, 30–33.
(17) Jiménez-Halla, C. O. C.; Fernandez, I.; Frenking, G. *Angew. Chem., Int. Ed.* **2009**, *48*, 366–369.
(18) Yockel, S.; Gawlik, E.; Wilson, A. K. *J. Phys. Chem. A* **2007**, *111*, 11261–11268.
(19) Jayasekharan, T.; Ghanty, T. K. *J. Chem. Phys.* **2008**, *129*, 184302/1–8.
(20) Wong, M. W. *J. Am. Chem. Soc.* **2000**, *122*, 6289–6290.
(21) (a) Runeberg, N.; Pettersson, M.; Khriachtchev, L.; Lundell, J.; Räsänen, M. *J. Chem. Phys.* **2001**, *114*, 836–841. (b) Khriachtchev, L.; Pettersson, M.; Lignell, A.; Räsänen, M. *J. Am. Chem. Soc.* **2001**, *123*, 8610–8611. (c) Khriachtchev, L.; Lignell, A.; Räsänen, M. *J. Chem. Phys.* **2004**, *120*, 3353–3357. (d) Pettersson, M.; Khriachtchev, L.; Lignell, A.; Räsänen, M.; Bihary, Z.; Gerber, R. B. *J. Chem. Phys.* **2002**, *116*, 2508–2515. (e) Lignell, A.; Khriachtchev, L.; Pettersson, M.; Räsänen, M. *J. Chem. Phys.* **2003**, *118*, 11120–11128. (f) Khriachtchev, A. L.; Räsänen, M.; Pettersson, M. *Chem. Phys. Lett.* **2004**, *390*, 256–260.
(22) (a) Bochenkova, A. V.; Khriachtchev, L.; Lignell, A.; Räsänen, M.; Lignell, H.; Granovsky, A. A.; Nemukhin, A. V. *Phys. Rev. B* **2008**, *77*, 094301/1–7. (b) Bochenkova, A. V.; Firsov, D. A.; Nemukhin, A. V. *Chem. Phys. Lett.* **2005**, *405*, 165–171.
(23) (a) Lundell, J.; Chaban, G. M.; Gerber, R. B. *Chem. Phys. Lett.* **2000**, *331*, 308–316. (b) Chaban, G. M.; Lundell, J.; Gerber, R. B. *J. Chem. Phys.* **2001**, *115*, 7341–7343. (c) Bihary, Z.; Chaban, G. M.; Gerber, R. B. *J. Chem. Phys.* **2002**, *117*, 5105–5108. (d) Chaban, G. M.; Lundell, J.; Gerber, R. B. *Chem. Phys. Lett.* **2002**, *364*, 628–633. (e) Bihary, Z.; Chaban, G. M.; Gerber, R. B. *J. Chem. Phys.* **2002**, *116*, 5521–5529. (f) Bihary, Z.; Chaban, G. M.; Gerber, R. B. *J. Chem. Phys.* **2003**, *119*, 11278–11284.
(24) (a) Berski, S.; Silvi, B.; Lundell, J.; Noury, S.; Latajka, Z. *Prog. Theor. Chem. Phys.* **2001**, *1*, 259–279. (b) Panek, J.; Latajka, Z.; Lundell, J. *Phys. Chem. Chem. Phys.* **2002**, *4*, 2504–2510.
(25) (a) McDowell, S. A. C. *Chem. Phys. Lett.* **2004**, *396*, 346–349. (b) McDowell, S. A. C. *J. Mol. Struct. (THEOCHEM)* **2004**, *674*, 227–232. (c) McDowell, S. A. C. *Mol. Phys.* **2004**, *102*, 71–77. (d) McDowell, S. A. C. *Chem. Phys.* **2004**, *301*, 53–60. (e) McDowell, S. A. C. *J. Chem. Phys.* **2004**, *120*, 3630–3634. (f) McDowell, S. A. C. *J. Mol. Struct. (THEOCHEM)* **2005**, *715*, 73–77. (g) McDowell, S. A. C. *Chem. Phys. Lett.* **2005**, *406*, 228–231. (h) McDowell, S. A. C. *Chem. Phys.* **2006**, *328*, 69–74. (i) McDowell, S. A. C.; Buckingham, A. D. *Theor. Chem. Acc.* **2008**, *119*, 29–34.
(26) (a) Takayanagi, T.; Wada, A. *Chem. Phys. Lett.* **2002**, *352*, 91–98. (b) Takayanagi, T. *Chem. Phys. Lett.* **2003**, *371*, 675–680.
(27) Wang, J.-T.; Feng, Y.; Liu, L.; Li, X.-S.; Guo, Q.-X. *Chem. Lett.* **2003**, *32*, 746–747.
(28) Jolkkonen, S.; Pettersson, M.; Lundell, J. *J. Chem. Phys.* **2003**, *119*, 7356.
(29) (a) Yen, S.-Y.; Mou, C.-H.; Hu, W.-P. *Chem. Phys. Lett.* **2004**, *383*, 606–611. (b) Chen, Y.-L.; Hu, W.-P. *J. Phys. Chem. A* **2004**, *108*, 4449–4454. (c) Li, T.-H.; Liu, Y.-L.; Lin, R.-J.; Yeh, T.-Y.; Hu, W.-P. *Chem. Phys. Lett.* **2007**, *434*, 38–41.
(30) (a) Solimannejad, M.; Alkorta, I. *Chem. Phys.* **2006**, *324*, 459–464. (b) Solimannejad, M.; Alkorta, I. *Chem. Phys. Lett.* **2007**, *439*, 284–287.
(31) Alabugin, I. V.; Manoharan, M.; Weinhold, F. A. *J. Phys. Chem. A* **2004**, *108*, 4720–4730.
(32) Avramopoulos, A.; Reis, H.; Li, J.; Papadopoulos, M. G. *J. Am. Chem. Soc.* **2004**, *126*, 6179–6184.
(33) Lein, M.; Frunzke, J.; Frenking, G. *Struct. Bonding (Berlin, Ger.)* **2004**, *106*, 181–191.
(34) Li, H.; Xie, D.; Guo, H. *J. Chem. Phys.* **2004**, *120*, 4273–4280.
(35) Huang, Z. G.; Xie, D. Q.; Zhu, H. *Sci. China, Ser. B: Chem.* **2007**, *50*, 7–10.
(36) Cukras, J.; Sadlej, J. *Chem. Phys. Lett.* **2008**, *459*, 44–48.
(37) Frisch, M. J.; Trucks, G. W.; Schlegel, H. B.; Scuseria, G. E.; Robb, M. A.; Cheeseman, J. R.; Montgomery, J. A., Jr.; Vreven, T.; Kudin, K. N.; Burant, J. C.; Millam, J. M.; Iyengar, S. S.; Tomasi, J.; Barone, V.; Mennucci, B.; Cossi, M.; Scalmani, G.; Rega, N.; Petersson, G. A.; Nakatsuji, H.; Hada, M.; Ehara, M.; Toyota, K.; Fukuda, R.; Hasegawa, J.; Ishida, M.; Nakajima, T.; Honda, Y.; Kitao, O.; Nakai, H.; Klene, M.; Li, X.; Knox, J. E.; Hratchian, H. P.; Cross, J. B.; Adamo, C.; Jaramillo, J.; Gomperts, R.; Stratmann, R. E.; Yazyev, O.; Austin, A. J.; Cammi, R.; Pomelli, C.; Ochterski, J. W.; Ayala, P. Y.; Morokuma, K.; Voth, G. A.; Salvador, P.; Dannenberg, J. J.; Zakrzewski, V. G.; Dapprich, S.; Daniels, A. D.; Strain, M. C.; Farkas, O.; Malick, D. K.; Rabuck, A. D.; Raghavachari, K.; Foresman, J. B.; Ortiz, J. V.; Cui, Q.; Baboul, A. G.; Clifford, S.; Cioslowski, J.; Stefanov, B. B.; Liu, G.; Liashenko, A.; Piskorz, P.; Komaromi, I.; Martin, R. L.; Fox, D. J.; Keith, T.; Al-Laham, M. A.; Peng, C. Y.; Nanayakkara, A.; Challacombe, M.; Gill, P. M. W.; Johnson, B.; Chen, W.; Wong, M. W.; Gonzalez, C.; Pople, J. A. *Gaussian 03*, revisions C.02 and D.02; Gaussian, Inc.: Wallingford, CT, 2004.
(38) (a) Dunning, T. H., Jr. *J. Chem. Phys.* **1989**, *90*, 1007–1023. (b) Woon, D. E.; Dunning, T. H., Jr. *J. Chem. Phys.* **1994**, *100*, 2975–2990. (c) Kendall, R. A.; Dunning, T. H., Jr.; Harrison, R. J. *J. Chem. Phys.* **1992**, *96*, 6796–6806. (d) Woon, D. E.; Dunning, T. H., Jr. *J. Chem. Phys.* **1993**, *98*, 1358–1371.
(39) Nicklass, A.; Dolg, M.; Stoll, H.; Preuss, H. *J. Chem. Phys.* **1995**, *102*, 8942–8952.
(40) Møller, C.; Plesset, M. S. *Phys. Rev.* **1934**, *46*, 618–622.
(41) Raghavachari, K.; Trucks, G. W.; Pople, J. A.; Head-Gordon, M. *Chem. Phys. Lett.* **1989**, *157*, 479–483.
(42) (a) Becke, A. D. *Phys. Rev. A* **1988**, *38*, 3098. (b) Becke, A. D. *ACS Symp. Ser.* **1989**, *394*, 165. (c) Becke, A. D. *J. Chem. Phys.* **1993**, *98*, 5648.
(43) Lee, C.; Yang, W.; Parr, R. G. *Phys. Rev. B* **1988**, *37*, 785–789.
(44) Gonzalez, C.; Schlegel, H. B. *J. Phys. Chem.* **1990**, *94*, 5523–5527.
(45) Glendening, E. D.; Reed, A. E.; Carpenter, J. E.; Weinhold, F. *NBO*, version 3.1; Theoretical Chemistry Institute, University of Wisconsin: Madison, WI (as implemented in Gaussian 03).
(46) Boys, S.; Bernardi, F. *Mol. Phys.* **1970**, *19*, 553–566.
(47) Bader, R. F. W. *Atoms in Molecules: A Quantum Theory*; Oxford University Press: Oxford, 1990.
(48) Biegler-König, F. *AIM2000*; University of Applied Sciences: Bielefeld, Germany, 2002 (http://www.AIM2000.de).
(49) Lee, T. J.; Taylor, P. R. *Int. J. Quantum Chem.* **1989**, *36*, 199–207.
(50) Lignell, A.; Khriachtchev, L.; Lundell, J.; Tanskanen, H.; Räsänen, M. *J. Chem. Phys.* **2006**, *125*, 184514.
(51) Koch, W.; Frenking, G.; Gauss, J.; Cremer, D.; Collins, J. R. *J. Am. Chem. Soc.* **1987**, *109*, 5917–5934.
(52) Grandinetti, F. *Int. J. Mass Spectrom.* **2004**, *237*, 243–267, and references therein.
(53) Li, T.-H.; Mou, C.-H.; Chen, H.-R.; Hu, W.-P. *J. Am. Chem. Soc.* **2005**, *127*, 9241–9245.
(54) Antoniotti, P.; Bronzolino, N.; Borocci, S.; Cecchi, P.; Grandinetti, F. *J. Phys. Chem. A* **2007**, *111*, 10144–10151.
(55) Cukras, J.; Sadlej, J. *Chem. Phys. Lett.* **2008**, *467*, 18–22, and references therein.
(56) The harmonic frequencies of $HHeFHeH^+$ calculated at the CCSD(T)/aug-cc-pVDZ and CCSD(T)/aug-cc-pVTZ levels of theory are quite similar to the MP2 estimates, with the largest differences of ca. 50−70 cm^{-1} in the wavenumbers of the H-Ng stretching modes. We also noticed a strict similarity between the MP2/aug-cc-pVTZ and B3LYP/aug-cc-pVTZ harmonic frequencies.
(57) The accuracy of the CCSD(T)/aug-cc-pVTZ/SDD//MP2/aug-cc-pVTZ/SDD energy estimates can be appreciated by comparing relevant thermochemical quantities calculated at this level with the corresponding experimental values (as quoted in ref 58). The theoretical dissociation energy, ionization energy, and PA of HF, 133.4 kcal mol^{-1}, 15.9 eV, and 115.4 kcal mol^{-1}, respectively, are nearly coincident with the experimental

values. The recombination energies of HNg^+ (with formation of H and Ng), computed as 11.8 (HHe^+), 11.5 (HNe^+), 9.7 (HAr^+), 9.1 (HKr^+), and 8.2 eV (HXe^+), favorably compare with the experimental values of 11.8, 11.5, 9.8, 9.2, and 8.4 eV, respectively. The theoretical PAs of Ng, computed as 42.0 (He), 49.3 (Ne), 90.9 (Ar), 104.7 (Kr), and 124.5 kcal mol^{-1} (Xe), respectively, show a slightly larger, but still fairly tolerable average deviation from the corresponding experimental values of 42.5, 47.5, 88.2, 101.5, and 119.4 kcal mol^{-1}.

(58) NIST Chemistry WebBook, NIST Standard Reference Database Number 69, June 2005 release. (http://webbook.nist.gov).

(59) Giordani, M.; Antoniotti, P.; Grandinetti, F. *Chem.—Eur. J.* **2010**, *16*, 6257−6264.

(60) The MP2/aug-cc-pVTZ/SDD single imaginary frequencies of **TS1** are 715.6i (Ng = He), 215.6i (Ng = Ne), 430.3i (Ng = Ar), 387.1i (Ng = Kr), and 342.9i cm^{-1} (Ng = Xe).

(61) The MP2/aug-cc-pVTZ/SDD single imaginary frequencies of **TS2** are 198.6i (Ng = Ar), 189.7i (Ng = Kr), and 167.6i cm^{-1} (Ng = Xe).

(62) Bent, H. *New Ideas in Chemistry from Fresh Energy for the Periodic Law*; AuthorHouse: Bloomington, IN, 2006.

(63) Scerri, E. R. *The Periodic Table: Its Story and Its Significance*; Oxford University Press: Oxford, U.K., 2007.

(64) Grochala, W. *Pol. J. Chem.* **2009**, *83*, 87–122.

JP102018N